transgene insertion did not grossly affect the function of the *Mctp1* gene.

To test whether the ectopic expression of EGFP reflected the expression of *Mctp1*, we performed in situ hybridization on E10.5 embryos with digoxigenin-labeled *Mctp1* probes. *Mctp1* expression was not detected specifically in the otocyst (data not shown). This result indicates that ectopic EGFP expression in the ear does not simply recapitulate *Mctp1* expression but may be a combinatory effect of the *Ednra* 5′-flanking region and some potential enhancer(s) within the *Mctp1* locus.

Morphological and functional integrity of Line-14 mice verified their utility as reporter mice to monitor inner ear development

To test the vestibular function of Line-14 mice, we performed the swim test for five homozygous mice, five heterozygous mice, and five wild-type controls. All the homozygous, heterozygous, and wild-type mice could swim with their heads above water for 60 seconds for three trials. To test the auditory function of Line-14 mice, we recorded ABR for the same test subjects (Fig. S6). There were no significant threshold differences among homozygous, heterozygous, and wild-type mice in each frequency according to the results of one-way ANOVA (Supporting Information Table S2). Homozygous and heterozygous mice tested for ABR had no morphological abnormality in hematoxylin and eosin staining (data not shown). These results revealed that adult Line-14 mice were morphologically and functionally intact, excluding the possible effect of the transgene-induced insertional mutation on vestibular and auditory functions. Given the spatiotemporal EGFP expression pattern and the spared morphology and function, Line-14 can be used as a reporter line to monitor differentiation into the pars inferior, including sensory patches, the endolymphatic duct, and the SAG.

Gene expression of the FACS-purified EGFP-positive cell population in E10.5 ventral and dorsomedial otocysts was profiled in microarray analysis

The microarray data in the present study were submitted to the Gene Expression Omnibus (GSE19618). To characterize EGFP-positive cells, we compared the gene expression profiles of FACS-sorted EGFP-positive and EGFP-negative cells from the otocysts of E10.5 transgenic embryos (Supporting Information Fig. S7). We confirmed that the EGFP sequence was amplified by real-time RT-PCR only in cDNA from the EGFP-positive cells (data not shown).

In total, 301 genes that were expressed in the E10.5 otocyst were acquired from the Gene Expression Literature Query Form and Gene Expression Data Query Form. We excluded 23 genes whose microarray data did not exist. Among the remaining 278 genes, 51, 202, and 25 genes matched the criteria for Group 1, Group 2, and Group 3, respectively (see Materials and Methods).

Microarray analysis is often performed to detect differentially expressed genes under different conditions. When attempting to detect these genes from microarray data, the efficiency of the ranking method for these genes is important. Therefore, we evaluated the performance of SLR for the prediction of genes expressed mainly in the ventral and/or dorsomedial otocyst, by using in situ hybridization data in the Gene Expression Literature Query Form and Gene Expression Data Query Form. The outcome was defined as genes matching the criteria of Group 1. Figure 5A shows the ROC curve; the AUC was 0.749 (95% confidence interval: 0.666–0.832). Figure 5B shows the number of genes in Group 1 (outcome), the

Figure 3. EGFP expression in the developing inner ear and the statoacoustic ganglion of Line-14 mice at E13.5 (A–F), E15.5 (G,H), P2 (I–N), and P9 (O,P). **A–C:** A section from the E13.5 ASCC in Line-14 mice (A,B) and its schematic view (C). EGFP expression was detected in ASCC hair cells, which was confirmed by double staining with GFP (green) and Myo7a (magenta). **D–F:** A section from the E13.5 saccule (D,E) and SAG in Line-14 mice and its schematic view (F). EGFP expression was detected in the saccule including hair cells, which was confirmed by double staining with GFP (green) and Myo7a (magenta). **G,H:** A section from the E15.5 cochlea basal turn in Line-14 mice. EGFP expression was detected in the cochlea including hair cells, which was confirmed by double staining with GFP (green) and Myo7a (magenta). The EGFP signals in the GER were stronger than those in the LER. **I–K:** Sections from the P2 LSCC in Line-14 mice. EGFP expression was detected in LSCC hair cells, which was confirmed by double staining with GFP (green) and Myo7a (magenta). EGFP expression was also detected in some LSCC supporting cells (bracket in K), which was confirmed by double staining with GFP (green) and $p27^{kip1}$ (magenta). **L–N:** Sections from the P2 cochlea in Line-14 mice. EGFP expression was detected in the GER and in the inner and outer hair cells, which was confirmed by double staining with GFP (green) and Myo7a (magenta) and in the inner phalangeal cells (arrow in N), which was confirmed by double staining with GFP (green) and $p27^{kip1}$ (magenta). **O,P:** A section from the P9 LSCC in Line-14 mice. EGFP expression was detected in LSCC hair cells, which was confirmed by double staining with GFP (green) and Myo7a (magenta). EGFP signals in some hair cells (bracket in O) weakened. See Supporting Information Figures S2–S5 for EGFP expression patterns in other regions of the inner ear. AC, anterior crista; ASCC, anterior semicircular canal; SM, saccular macula; SAG, statoacoustic ganglion; CD, cochlear duct; GER, greater epithelial ridge; LER, lesser epithelial ridge; LC, lateral crista; OC, organ of Corti; D, dorsal; L, lateral. Scale bar = 20 μm in A,B,D,E, I–P; 50 μm in G,H.

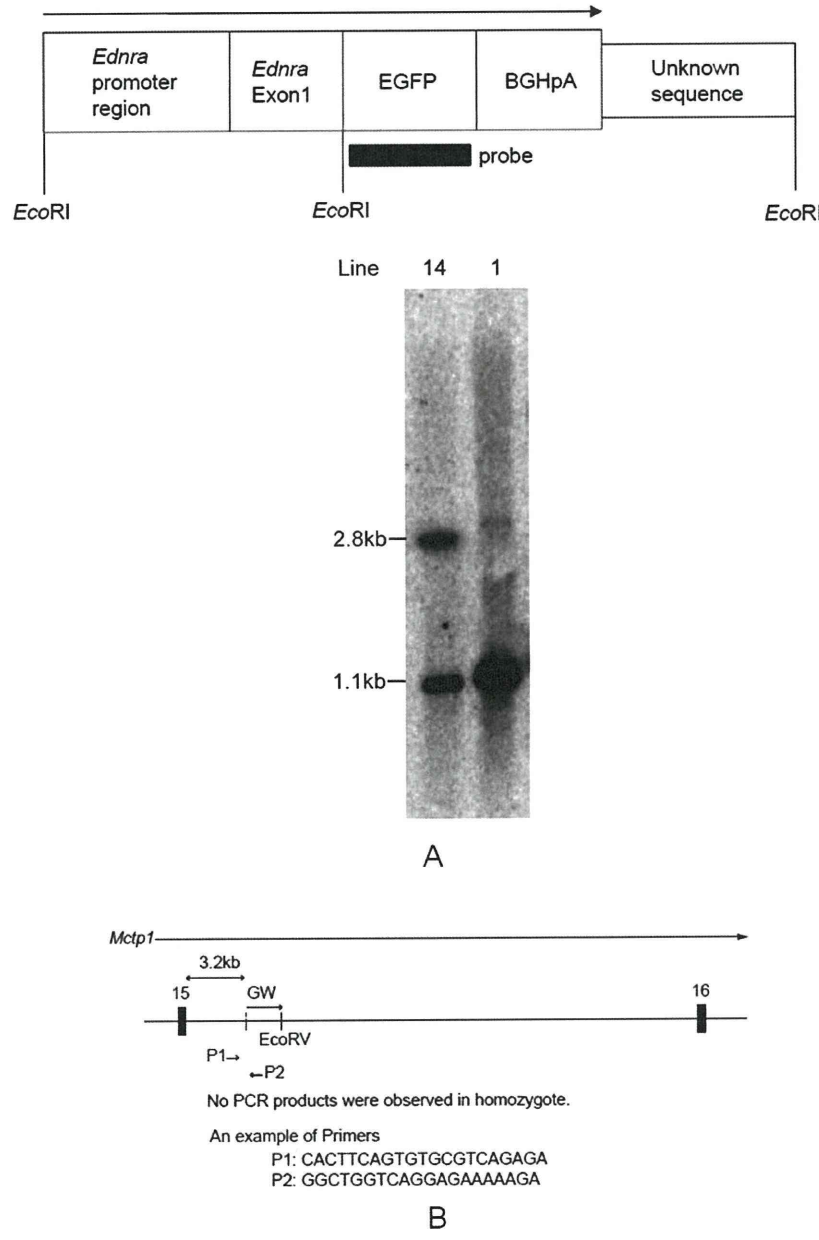

Figure 4. Southern blot analysis and genome walking analysis of the genomic regions surrounding the transgene integrated loci in Line-14 mice. **A:** Autoradiographs shown in the panels above were probed with the 657-bp EGFP sequence. The probe hybridized to a band of ~1.1 kb in *Eco*RI-digested DNA from Line-1 mice. Hybridization to DNA derived from Line-14 mice localized to the ~1.1-kb band and to another band that migrated at ~2.8 kb. The ~2.8-kb band was considered to encompass the genomic DNA/transgene transition in Line-14 mice. **B:** The schematic view of the candidate transgene-genomic junction located at the intronic regions of the *Mctp1* gene. Genomic PCR for a homozygous mouse, whose primers were designed at the *Mctp1* sequence to straddle the junction, showed no bands. GW, sequence detected by the genome walking method.

number of genes in Group 3, and the positive predictive value (PPV) corresponding to the cutoff value of SLR. When the cutoff value of SLR was set at ≥ 1.3, no Group 3 genes were found. When the cutoff value was set at 1.3, the sensitivity, specificity, and PPV were 37%, 96%, and 68%, respectively. The PPV at 1.3 was higher than that at 1.7. We set the optimal cutoff value of SLR at 1.3 in the following analyses.

Considering the above result, we defined the criteria for the genes selectively expressed in EGFP-positive cells

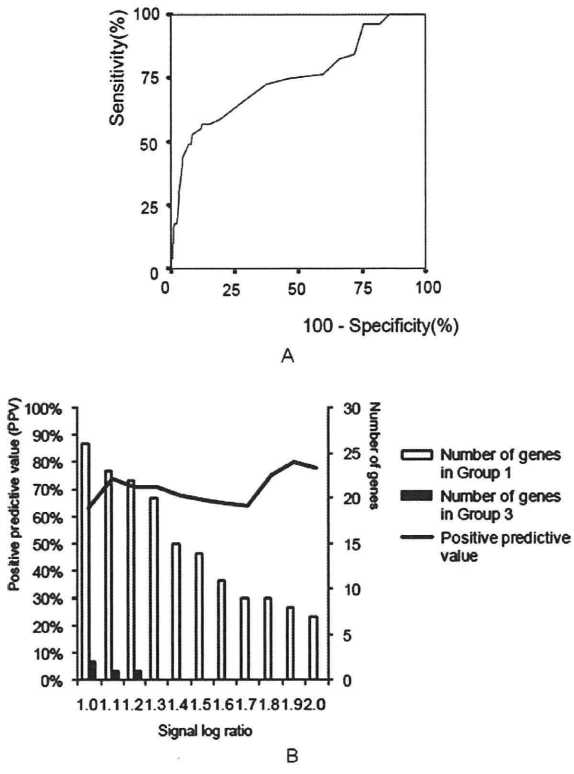

Figure 5. Evaluation of the performance of SLR as a predictor of gene expression mainly in the ventral and/or dorsomedial otocyst. **A:** ROC curves for SLR. The outcome was defined as a gene belonging to Group 1. Sensitivity represented the [number of true-positive subjects]/[(number of true-positive subjects) + (number of false-negative subjects)] calculated at each cutoff value. Specificity represented the [number of true-negative subjects]/[(number of true-negative subjects) + (number of false-positive subjects)] calculated at each cutoff value. The AUC was 0.749 (95% confidence interval, 0.666–0.832). **B:** The number of genes in Group 1 (outcome), the number of genes in Group 3, and the PPV corresponding to the cutoff value of SLR. When the cutoff value of SLR was set at $\geq$1.3, no Group 3 genes were found. When the cutoff value was set at 1.3, the PPV was 71%, which was higher than that at 1.7.

as follows: 1) the detection calls were present in EGFP-positive cells; 2) the changed *P* values were $\leq$0.003; and 3) the SLRs were $\geq$1.3. When these criteria were adopted, the sensitivity, specificity, and PPV were 35%, 96%, and 69%, respectively. By using these criteria, we identified 265 genes that showed higher expression in EGFP-positive cells than in EGFP-negative cells. Table 2 shows the top 32 genes (SLR > 2.5) that showed higher expression in EGFP-positive cells. Among the 265 genes enriched in EGFP-positive cells, 26 (10%) were expressed in the otocyst and 19 (7%) showed regional-specific expression patterns. Moreover, all the genes were mainly expressed in the ventral and/or dorsomedial region (Table 3). Notably, 18 (7%) genes enriched in EGFP-positive cells have been implicated in ear development in mice (Table 4) and/or human diseases involving the inner ear (Table 5).

We performed functional analysis of significantly regulated genes, as identified by microarray, by using the OntoExpress software. Statistically enriched biological categories of the pool of genes in the microarray were calculated and listed according to their quantitative representation of total genes. Analysis of biological processes revealed that genes involved in the regulation of development, including that of the inner ear, were preferentially enriched in EGFP-positive regions (Table 6) . Analysis of cellular components revealed that genes that are more highly expressed in EGFP-positive cells were preferentially located in cell junctions, including tight junctions (Table 6).

Validity of the microarray analysis was confirmed by RT-PCR

To confirm the validity of the microarray analysis, we monitored the relative expression levels of representative markers that were changed by using RT-PCR. Particularly, we mainly selected transcription factor genes involved in regional identity to demarcate the EGFP-positive region. In the microarray analysis, the SLRs of *Otx1* and *Otx2* displayed the highest levels of relative increase in EGFP-positive cells. Consistently, RT-PCR detected *Otx1* and *Otx2* expression only in EGFP-positive cells (Fig. 6A). At E10.25, *Otx1* was detected in the ventrolateral wall of the otocyst, whereas *Otx2* was detected in the ventral tip of the otocyst (Morsli et al., 1999). Throughout the developmental process, *Otx1* was expressed in a region destined to form the lateral SCC (LSCC), lateral crista, utricle, and pars inferior, whereas *Otx2* was expressed mostly in the region destined to form the pars inferior (Morsli et al., 1999). The function of *Prr15* in the inner ear is unknown; however, it has been previously reported that the gene is expressed in the ventral region of the E10.5 otocyst (Meunier et al., 2003). *Prr15* was increased in EGFP-positive cells both in microarray and RT-PCR (Fig. 6A). *Gbx2*, a marker of the dorsomedial region of the otocyst (Wassarman et al., 1997), was also increased in EGFP-positive cells both in microarray and RT-PCR (Fig. 6A). In contrast, *Prrx2*, a marker of the dorsolateral region of the otocyst (ten Berge et al., 1998; Beverdam and Meijlink, 2001), was shown to be downregulated in EGFP-positive cells by RT-PCR as well as the microarray analysis (Fig. 6A).

We then selected some genes that are considered to be markers of a presumptive neurosensory domain of the otocyst for RT-PCR analysis. From the list of genes unchanged in microarray (SLR $\leq$ 1.2), we selected *Isl1*, a marker of cells that will develop either as SAG

TABLE 2.

Top 32 (signal log ratio > 2.5) genes more expressed in EGFP-positive cells

Gene	Symbol	Signal log ratio	Signal of GFP-positive cells
orthodenticle homolog 1 (Drosophila)	*Otx1*	7.6	162.9
orthodenticle homolog 2 (Drosophila)	*Otx2*	5.9	225.5
membrane targeting (tandem) C2 domain containing 1	*Tc2n*	5	20.9
peptidy1 arginine deiminase, type III	*Padi3*	4.9	17
RIKEN cDNA 5430433G21 gene		4.8	8
RAR-related orphan receptor beta	*Rorb*	4.8	35
leucine rich repeat containing 8 family, member E	*Lrrc8e*	4.7	17.3
cDNA sequence BC060267		4.7	17.5
fibronectin leucine rich transmembrane protein 3	*Flrt3*	4.5	6.6
cDNA sequence BC055107		4.5	40.6
zinc finger protein 533	*Zfp385b*	4.4	47.2
Hedgehog-interacting protein	*Hhip*	3.9	17.6
RIKEN cDNA 1600029D21 gene		3.9	22.1
Hypothetical protein LOC668215		3.5	6.4
gamma-aminobutyric acid (GABA-A) receptor, subunit epsilon	*Gabre*	3.3	15.2
empty spiracles homolog 2 (Drosophila)	*Emx2*	3.3	100.5
proline rich 15	*Prr15*	3.2	244
solute carrier family 27 (fatty acid transporter), member 2	*Slc27a2*	3.2	61.5
regulator of G-protein signaling 13	*Rgs13*	3.1	99.8
zinc finger, DHHC domain containing 23	*Zdhhc23*	3.1	25.9
RIKEN cDNA 9930013L23 gene		3.1	157.9
aldehyde dehydrogenase family 1, subfamily A3	*Aldh1a3*	3.1	15.7
RIKEN cDNA 9430021M05 gene		2.8	22
calmodulin-like 4	*Calml4*	2.7	59.8
RAB20, member RAS oncogene family	*Rab20*	2.7	19
gastrulation brain homeobox 2	*Gbx2*	2.7	580.3
carboxylesterase 3	*Ces3*	2.6	53.5
kelch-like 14 (Drosophila)	*Klhl14*	2.6	181.2
leukocyte cell derived chemotaxin 1	*Lect1*	2.6	878.3
matrilin 1, cartilage matrix protein 1	*Matn1*	2.6	26.8
protocadherin 15	*Pcdh15*	2.6	39
espin	*Espn*	2.6	91.6

TABLE 3.

List of the genes enriched in EGFP-positive cells whose expression in E10.5 otocyst was confirmed by *in situ* hybridization

Mainly Ventral otocyst									
Aldga1a3	*Bdnf*	*Eya1*	*Foxg1*	*Gata3*	*Gli1*	*Lfng*	*Lrig1*	*Myo7a*	*Neurod1*
Neurog1	*Otx1*	*Otx2*	*Pdgfa*	*Prr15*	*Sall1*	*Six1*			
Mainly Dorsomedial otocyst									
Gbx2	*Sp5*								
Otocyst (no clear regional specificity)									
Cldn6	*Emx2*	*Eya4*	*Lmo7*	*Lmx1a*	*Pcdh19*	*Ripk4*			

neuroblasts or hair cell progenitors (Li et al., 2004; Radde-Gallwitz et al., 2004); *Bmp4*, a marker of cells that will develop as sensory progenitors in the SCCs (Wu and Oh, 1996; Morsli et al., 1998); *Jag1*, a marker of cells that will develop as progenitor cells that give rise to both hair cells and supporting cells (Kiernan et al., 2006); and *Sox2*. From the list of genes that showed higher expression in GFP-positive cells in the microarray (SLR $\geq$ 1.3), we selected *Lfng*, a marker of both neurogenic regions of the otocyst and prosensory regions destined to form the cochlea and the otolith organs (Morsli et al., 1998; Ozaki et al., 2004; Bok et al., 2007) and *Neurog1*, a marker of cells that will develop as SAG neuroblasts (Raft et al., 2007). RT-PCR confirmed that *Isl1*, *Bmp4*, *Jag1*, and *Sox2* were similarly expressed in both the EGFP-positive and EGFP-negative regions (Fig. 6A). As for *Bmp4*, the expresson in EGFP-negative cells was slightly dominant. *Lfng* and *Neurog1*were expressed in both the EGFP-positive and EGFP-negative regions (Fig. 6A). These results indicate that EGFP expression demarcates the ventral and dorsomedial regions within the E10.5 otocysts and includes sensory and neural progenitors, whereas the EGFP-negative population also includes sensory and neural progenitors.

TABLE 4.

List of the genes enriched in EGFP-positive cells whose knockout mice have phenotype in the ear

Symbol	Signal log ratio	Signal of GFP-positive cells	Phenotype of knockout mouse in the ear
Otx1	7.6	162.9	Absence of the LSCC, the lateral crista, the utriculosaccular duct and the cochleosaccular duct. Malformed cochlear hook and defects in the shape of the pars inferior.
Otx2	5.9	225.5	*Otx1* (−/−)/*Otx2* (+/−) compound mutants: More severe phenotype, particularly in ventral structures, including the saccule and cochlea, than *Otx1* (−/−).
Emx2	3.3	100.5	Abnormal middle ear ossicle morphology. In heterozygote, increased cochlear hair cell number.
Gbx2	2.7	580.3	Absent endolymphatic duct. Absent or abnormal cochlear and vestibular labyrinth.
Espn	2.6	91.6	Shortening of hair cell stereocilia. Degeneration of both inner and outer hair cells. Severe deafness and vestibular dysfunction.
Myo7a	2.1	296.3	Deafness, head-shaking, and circling with degeneration of the organ of Corti, spiral ganglion, stria vascularis in the cochlea, and vestibular ganglion in the labyrinth.
Bdnf	1.8	109.3	Abnormal cochlear outer hair cell afferent innervation. Abnormal type I vestibular cell. Abnormal crista.
Eya4	1.8	363.9	Abnormal middle ear morphology. Increased susceptibility to otitis media.
Clrn1	1.6	58.8	Progressive hearing loss and loss of balance. Defects in cochlear outer hair cells and supporting cells.
Fbxo2	1.6	197.8	Accelerated, age-related hearing loss associated with cochlear degeneration.
Lymx1a	1.6	373.6	Absent or malformed cochlea. Undeveloped SCCs.
Eya1	1.5	262.1	Severe malformations in the outer, middle and inner ear. Arrest of inner ear development at otocyst stage. Absent facioacoustic ganglion. Absent or malformed endolymphatic duct.
Gata3	1.5	201.7	Cystic inner ear with a single extension of the endolymphatic duct and no formation of SCCs or saccular and utricular recesses.
Otog	1.5	98.7	Progressive hearing loss and loss of balance. Abnormal tectorial membrane of the organ of Corti, otolith organs, and crista of SCCs.
Six1	1.4	599.6	Abnormal otocyst development. Absent cochlea. Abnormal vestiubular organs and endolymphatic duct.
Foxg1	1.3	754.5	Shortened cochlea with multiple rows of hair cells and supporting cells. Lacking horizontal crista. Malformed SCCs. Abnormal cochlear and vestibular innervations.
Neurod1	1.3	1432.4	Failure of inner ear sensory neuron survival during development.
Neurog1	1.3	216.7	Loss of sensory neurons and hair cells.

TABLE 5.

List of the genes enriched in EGFP-positive cells that are implicated in human diseases involving the inner ear

Symbol	Signal log ratio	Signal of GFP-positive cells	Human diseases related to the inner ear (OMIM ID)
Espn	2.6	91.6	DFNB36 (609006)
Myo7a	2.1	296.3	Usher syndrome type 1B (276900), DFNA11 (601317), DFNB2 (600060)
Eya4	1.8	363.9	DFNA10 (601316)
Marveld	1.6	180.3	DFNB49 (610153)
Clrn1	1.6	58.8	Usher syndrome type 3 (276902)
Eya1	1.5	262.1	branchiootorenal syndrome 1 (113650)
Gata3	1.5	201.7	hypoparathyroidism, sensorineural deafness, and renal disease (146255)

DFNA: autosomal dominant non-syndromic deafness, DFNB: autosomal recessive non-syndromic deafness

Among the genes showing increased expression that are known to be causative factors for human diseases of the inner ear (Table 5), we investigated the expression of five representative genes: *Espn*, *Myo7a*, *Eya4*, *Eya1*, and *Gata3*. In the EGFP-positive region, the dominant expression of these genes in EGFP-positive cells was confirmed by RT-PCR (Fig. 6B).

We aimed to confirm the validity of the microarray analysis for the genes enriched in EGFP-positive cells whose expression in the murine E10.5 otocyst has not been reported previously. From the genes enriched in EGFP-positive cells, we selected the genes according to the following criteria: 1) no reported expression in murine E10.5 otocyst, and 2) a relatively higher value in signal (>150).

TABLE 6.

List of GO terms whose FDR corrected P value was significantly higher in GO analysis of the genes enriched in EGFP-positive cells

GO terms	Corrected P-value	Number of genes
Biological Process		
inner ear morphogenesis	$<1\times10^{5}$	9
multicellular organismal development	<0.001	30
ureteric bud development	<0.01	5
homophilic cell adhesion	<0.05	6
ureteric bud branching	<0.05	4
neuron differentiation	<0.05	5
regulation of transcription	<0.05	15
cell adhesion	<0.05	14
anatomical structure development	<0.05	3
tumor necrosis factor-mediated signaling pathway	<0.05	2
inner ear development	<0.05	3
Cellular Component		
tight junction	$<1\times10^{7}$	11
cell junction	$<1\times10^{5}$	18
extracellular region	<0.001	33
plasma membrane	<0.001	39
membrane	<0.001	85
apical plasma membrane	<0.01	6
proteinaceous extracellular matrix	<0.01	11
sarcolemma	<0.01	4
basement membrane	<0.05	5
apical part of cell	<0.05	4
integral to plasma membrane	<0.05	9

FDR = False discovery rate, GO = Gene Ontology

One hundred twenty-nine genes fulfilled these criteria. Among these 129 genes, by using Onto-Express, we aimed to choose those that belonged to statistically enriched biological categories in the pool of genes in the microarray. We targeted genes involved in the regulation of multicellular organismal development (GO ID: GO:0007275) in the analysis of the biological process, and thus chose nine genes. From these nine genes, we finally selected two genes that had relatively higher values in the SLR (>2.0): *Lect1* and *Tnfrsf12a*. *Lect1*, a synonym for chondromodulin-1 (*chm1*), encodes a glycoprotein that stimulates the growth of chondrocytes and inhibits angiogenesis (Hiraki et al., 1997). In medaka, *chm1* was expressed in the otocyst and later exclusively in the SCC (Nemoto et al., 2008). *Tnfrsf12a*, a synonym for fibroblast growth factor-inducible-14 (*Fn14*), is located in the plasma membrane and is involved in cell-matrix interactions (Meighan-Mantha et al., 1999). In the EGFP-positive region, the dominant expression of these genes was also confirmed by RT-PCR (Fig. 6C).

DISCUSSION

The *Ednra-EGFP* Line-14 transgenic line is a novel line expressing EGFP in the placode-derived inner ear sensory cell lineage. At E10.5, EGFP expression was detected in the ventral and dorsomedial regions of the otocyst. By combining this line with FACS-array technology, we performed gene expression profiling focusing on the regional specificity of the otocyst. EGFP expression patterns in Line-14 based on immunohistochemistry and RT-PCR data are summarized in Figure 7.

In mice, morphogenesis of the otocyst starts with an evagination of the epithelium on the dorsomedial side (Kaufman and Bard, 1999; Kiernan et al., 2002). This bud of the endolymphatic duct and sac elongates dorsally. After the appearance of the endolymphatic bud, the ventral region of the otocyst begins to elongate in a ventral direction, initiating cochlear development (Kaufman and Bard, 1999; Kiernan et al., 2002). The saccule and its macula are not distinguishable at E12; however, at E13, they are located ventral to the utricle and close to the beginning of the first turn of the cochlea (Morsli et al., 1998). In Line-14, EGFP expression was detected in the ventral and dorsomedial regions of the otocyst at E10.5, and delamination of EGFP-positive neural-fated cells from the otic epithelium that would form SAG neurons was observed. When the otocyst almost transformed into the labyrinth at E12.5, continuous EGFP expression was observed in the cochlea, saccule, and endolymphatic duct.

In contrast, EGFP expression was also detected in hair cells in the pars superior, but the spatiotemporal continuity of EGFP expression from the otocyst was not detected. In the microarray analysis, *Otx1* and *Otx2* displayed the highest levels of relative increase in EGFP-positive cells (Table 2). The RT-PCR findings also support the regional-specific expression patterns of *Otx1*, *Otx2*, and *Gbx2* in EGFP-positive cells (Fig. 6A). These EGFP expression patterns and discriminative findings of both microarray and RT-PCR imply that the EGFP-positive region at E10.5 could include the region destined for the LSCC including the crista, the utricle including the macula, the pars inferior including the sensory patches, the endolymphatic duct, and SAG neuroblasts, and might partially include the prosensory anlagen of the anterior and posterior cristae. The region might also have the potential to give rise to the sensory patches in the pars superior, although it could not be confirmed whether the EGFP-positive hair cells in the pars superior migrated from the EGFP-positive region at E10.5.

Ednra, whose promoter was used for the integrated transgene in the present study, is not directly involved in the development of the inner ear. Therefore, we speculated that a certain gene related to inner ear development and sensory cell differentiation at the chromosomal integration site might be responsible for this ectopic EGFP expression. Other positional effects at the transgene integration locus should also be considered as causative factors for ectopic expression. In the present study, we

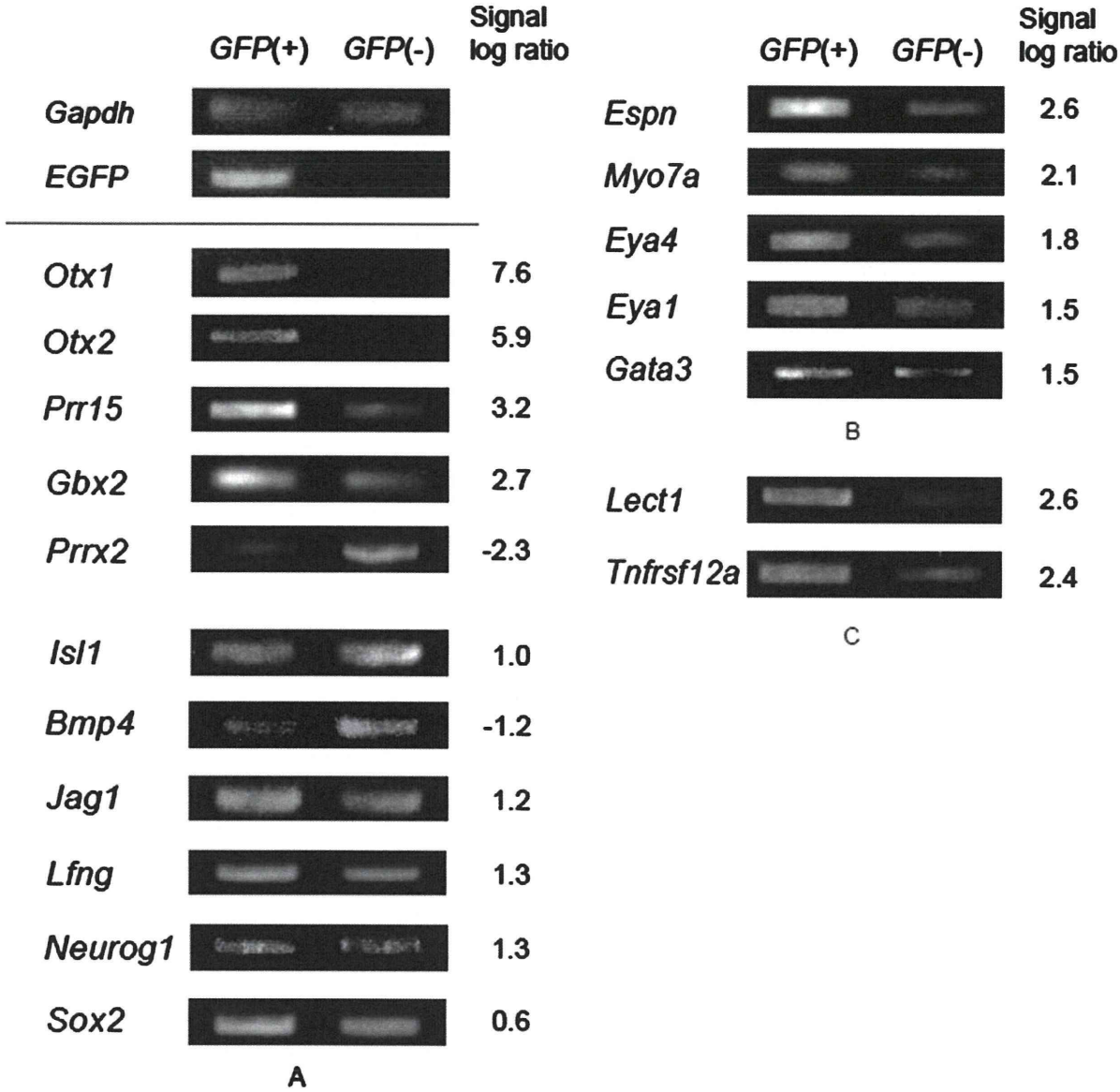

Figure 6. RT-PCR analysis of EGFP-positive and EGFP-negative cells. **A:** RT-PCR analysis of marker genes for specific regions in the otocyst and developing inner ear cell types. EGFP-positive cells in the E10.5 otocyst expressed markers of the ventral region of the otocyst (*Otx1* and *Otx2*) which was not detected in EGFP-negative cells. *Prr15*, a gene that is expressed in the ventral region of the E10.5 otocyst but whose function is unknown, was expressed dominantly in EGFP-positive cells. *Gbx2*, a representative dorsomedial marker of the otocyst, was expressed dominantly in EGFP-positive cells. *Prrx2*, a representative dorsolateral marker of the otocyst, was expressed dominantly in EGFP-negative cells. EGFP-positive cells also included sensory (*Isl1*, *Bmp4*, *Jag1*, *Lfng*, and *Sox2*) and neural (*Neurog1*, *Lfng*, and *Sox2*) progenitors. **B:** RT-PCR analysis of the five representative genes enriched in EGFP-positive cells that are implicated in human diseases of the inner ear: *Espn*, *Myo7a*, *Eya4*, *Eya1*, and *Gata3*. The dominant expression of these five genes in EGFP-positive cells was confirmed. **C:** RT-PCR analysis of the two representative genes enriched in EGFP-positive cells that were involved in the regulation of multicellular organismal development in analyses of biological processes by Onto-express: *Lect1* and *Tnfrsf12a*. The dominant expression of these two genes in GFP-positive cells was confirmed.

demonstrate that the transgene was inserted into the intronic region of the *Mctp1* gene. MCTPs (multiple C2 domain and transmembrane region proteins) are a family of evolutionarily conserved C2 domain proteins with unusual Ca^{2+}-dependent properties, and *Mctp1* is one of the two MCTP genes expressed in vertebrates (Shin et al., 2005). As shown above, we could not completely elucidate how the transgenic constructions were integrated in

Line-14; moreover, we could not identify the chromosomal sequence responsible for the ectopic expression in the developing inner ear in Line-14. Further studies are required to determine the mechanism of this ectopic expression.

In the present study, we compared the gene expression profiles of EGFP-positive cells and EGFP-negative cells derived from the E10.5 otocyst. Sampling of the FACS-purified EGFP-positive cell populations allowed regional-specific gene expression profiling in the otocyst. We evaluated the performance of the SLR for the prediction of genes expressed mainly in the ventral and/or dorsomedial otocyst. The outcome was defined as a gene belonging to Group 1. For the SLR of microarray data, the AUC was calculated. By showing the number of genes in Group 1 (outcome), the number of genes in Group 3, and the PPV corresponding to the cutoff value of SLR, we objectively demonstrated the predictive performance of the gene expression profile in the present study. With regard to the in situ hybridization data from the GXD database, most of the genes in Group 2 were attributed to the findings of whole-mount in situ hybridization, for which it was difficult to determine the regional specificity of expression patterns.

The regional specificity of these genes in the ventral and/or dorsomedial region may be demonstrated in the future. If the intended genes were confined to the genes in Groups 1 and 3, both of which had regional-specific expression patterns, the specificity was 100% on the condition that the SLR was ≥ 1.3. This profile could be helpful as a tool for narrowing the number of unknown genes that may have regional-specific expression patterns. The statistical methods for gene expression analyses by using microarray have been recently assessed from the viewpoint of sensitivity, specificity, and reproducibility. In a comparison between two groups in a Affymetrix GeneChip study, optimal gene ranking methods have been suggested (Shi et al., 2006; Kadota et al., 2009). In the

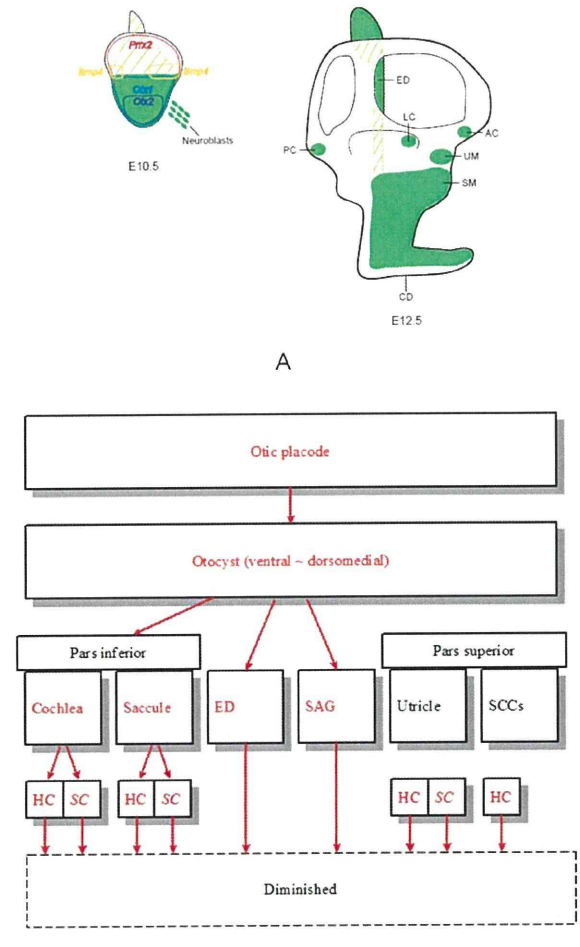

Figure 7

Figure 7. Summary of EGFP expression patterns in the developing inner ear of Line-14 mice based on immunohistochemistry and RT-PCR data. **A:** Schematic views from the lateral side of the inner ear at E10.5 and E12.5. At E10.5, EGFP expression (green) was detected in the ventral and dorsomedial regions of the otocyst. We selected *Otx1* and *Otx2* as markers of the ventral region of the otocyst, and *Prrx2* as a marker of the dorsolateral region of the otocyst. *Otx1* (light blue) and *Otx2* (dark blue) were expressed in the EGFP-positive region but not in the EGFP-negative region. *Prrx2* (magenta) was dominantly expressed in the EGFP-negative region. At E12.5, in the pars inferior, this line retained the spatiotemporal continuity of EGFP expression from the otocyst to sensory hair cells. Apart from the continuing EGFP-positive region, EGFP-positive hair cells were located in each SCC crista and the utricular macula. **B:** Summary of spatiotemporal EGFP expression patterns in the developing inner ear of Line-14 mice. EGFP expression was first detected at E8.5–9.0 in the otic placode. At E10.5, EGFP expression was detected in the ventral and dorsomedial regions of the otocyst. In the pars inferior, this line retained the spatiotemporal continuity of EGFP expression from the otocyst to sensory hair cells. In contrast, in the sensory hair cells of the pars superior, the spatiotemporal continuity of EGFP expression from the otocyst was not observed; it was likely that these hair cells expressed EGFP at certain degrees of differentiation. As the differentiation into the inner ear sensory patches progressed, EGFP expression was restricted to hair cells and some of the supporting cells in the sensory patches; it gradually diminished with the advance of morphological maturity. AC, anterior crista; LC, lateral crista; PC, posterior crista; UM, utricular macula; SM, saccular macula; CD, cochlear duct, ED, endolymphatic duct; ASCC, anterior semicircular canal; LSCC, lateral semicircular canal; PSCC, posterior semicircular canal; SAG, statoacoustic ganglion; HC, hair cells; *SC*, some of the supporting cells.

present study, the reproducibility was not evaluated; moreover, no comparison with other methods was performed with regard to the sensitivity and specificity. However, by using FACS-array technology with the novel EGFP reporter mice, we objectively demonstrated the conformity of the gene expression profile with known gene expression patterns in the otocyst. The method used here is expected to establish a basis for the construction of appropriate algorithms in transcriptome analysis of inner ear development.

Most of the genes enriched in EGFP-positive cells whose expression in the otocyst has not been reported were discovered, whereas many known and expected genes were also identified (Table 3). At E10.5, the EGFP-positive region mainly included the region destined to be the pars inferior and the endolymphatic duct. Many known genes implicated in murine ear development were identified from the genes enriched in the GFP-positive cells (Table 4). From the viewpoint of the analysis of the biological process in GO analysis, as we expected, the genes involved in the regulation of development were preferentially enriched in EGFP-positive regions (Table 6). These data could be mined to uncover many novel genes involved in inner ear morphogenesis and cell fate regulation. Additionally, some of the genes with increased expression in EGFP-positive cells have been known to cause human diseases involving the inner ear (Table 5). These data suggest that some novel genes enriched in EGFP-positive regions may be potentially involved in human congenital sensorineural hearing loss.

In conclusion, we established a novel transgenic mouse line expressing EGFP in the placode-derived inner ear sensory cell lineage. At E10.5, EGFP expression was detected in the ventral and dorsomedial regions of the otocyst. By combining this reporter line with FACS-array technology, we developed a gene expression profile specifically for the regional specificity of the otocyst. EGFP-positive regions included the *Otx1*-positive region, which could be clearly distinguished from EGFP-negative regions. The SLR of microarray data showed high performance for predicting genes expressed mainly in the ventral and/or dorsomedial otocyst, and could be mined to uncover many novel genes involved in inner ear morphogenesis and cell fate regulation. Additionally, these data suggest that some novel genes enriched in EGFP-positive regions may be potentially involved in human congenital sensorineural hearing loss. This reporter line could play important roles in the use of animal models for the analysis of the differentiation of the prosensory region into sensory patches, and the identification of regional-specific gene networks and novel gene functions in the developing inner ear.

ACKNOWLEDGMENTS

We thank all the technicians and colleagues who helped with our work. We also thank Dr. Yoshiro Ishimaru, a project assistant professor at Taste Science, Department of Applied Biological Chemistry, Graduate School of Agricultural and Life Sciences, for kind advice on technical problems.

LITERATURE CITED

Ashburner M, Ball CA, Blake JA, Botstein D, Butler H, Cherry JM, Davis AP, Dolinski K, Dwight SS, Eppig JT, Harris MA, Hill DP, Issel-Tarver L, Kasarskis A, Lewis S, Matese JC, Richardson JE, Ringwald M, Rubin GM, Sherlock G. 2000. Gene ontology: tool for the unification of biology. The Gene Ontology Consortium. Nat Genet 25:25–29.

Benjamini Y, Hochberg Y. 1995. Controlling the false discovery rate: a practical and powerful approach to multiple testing. J R Stat Soc Ser B 57:289–300.

Bermingham-McDonogh O, Oesterle EC, Stone JS, Hume CR, Huynh HM, Hayashi T. 2006. Expression of Prox1 during mouse cochlear development. J Comp Neurol 496: 172–186.

Beverdam A, Meijlink F. 2001. Expression patterns of group-I aristaless-related genes during craniofacial and limb development. Mech Dev 107:163–167.

Bok J, Chang W, Wu DK. 2007. Patterning and morphogenesis of the vertebrate inner ear. Int J Dev Biol 51:521–533.

Carney PR, Silver J. 1983. Studies on cell migration and axon guidance in the developing distal auditory system of the mouse. J Comp Neurol 215:359–369.

Chen P, Segil N. 1999. p27(Kip1) links cell proliferation to morphogenesis in the developing organ of Corti. Development 126:1581–1590.

Chen ZY, Corey DP. 2002. An inner ear gene expression database. J Assoc Res Otolaryngol 3:140–148.

Draghici S, Khatri P, Bhavsar P, Shah A, Krawetz SA, Tainsky MA. 2003. Onto-Tools, the toolkit of the modern biologist: Onto-Express, Onto-Compare, Onto-Design and Onto-Translate. Nucleic Acids Res 31:3775–3781.

Favaro R, Valotta M, Ferri AL, Latorre E, Mariani J, Giachino C, Lancini C, Tosetti V, Ottolenghi S, Taylor V, Nicolis SK. 2009. Hippocampal development and neural stem cell maintenance require *Sox2*-dependent regulation of Shh. Nat Neurosci 12:1248–1256.

Fekete DM, Muthukumar S, Karagogeos D. 1998. Hair cells and supporting cells share a common progenitor in the avian inner ear. J Neurosci 18:7811–7821.

Hasson T, Heintzelman MB, Santos-Sacchi J, Corey DP, Mooseker MS. 1995. Expression in cochlea and retina of myosin VIIa, the gene product defective in Usher syndrome type 1B. Proc Natl Acad Sci U S A 92:9815–9819.

Hasson T, Gillespie PG, Garcia JA, MacDonald RB, Zhao Y, Yee AG, Mooseker MS, Corey DP. 1997. Unconventional myosins in inner-ear sensory epithelia. J Cell Biol 137: 1287–1307.

Hiraki Y, Inoue H, Iyama K, Kamizono A, Ochiai M, Shukunami C, Iijima S, Suzuki F, Kondo J. 1997. Identification of chondromodulin I as a novel endothelial cell growth inhibitor. Purification and its localization in the avascular zone of epiphyseal cartilage. J Biol Chem 272:32419–32426.

Kadota K, Nakai Y, Shimizu K. 2009. Ranking differentially expressed genes from Affymetrix gene expression data: methods with reproducibility, sensitivity, and specificity. Algorithms Mol Biol 4:7.

Kaufman MH, Bard JBL. 1999. The eye and the ear. In: The anatomical basis of mouse development. San Diego: Academic Press. p194–208.

Kelley MW, Talreja DR, Corwin JT. 1995. Replacement of hair cells after laser microbeam irradiation in cultured organs of corti from embryonic and neonatal mice. J Neurosci 15: 3013–3026.

Khan Z, Carey J, Park HJ, Lehar M, Lasker D, Jinnah HA. 2004. Abnormal motor behavior and vestibular dysfunction in the stargazer mouse mutant. Neuroscience 127:785–796.

Kiernan AE, Steel KP, Fekete DM. 2002. Development of the mouse inner ear. In: Rossant J, Tam PL, editors. Mouse development: patterning, morphogenesis and organogenesis. San Diego: Academic Press. p539–566.

Kiernan AE, Xu J, Gridley T. 2006. The Notch ligand JAG1 is required for sensory progenitor development in the mammalian inner ear. PLoS Genet 2:e4.

Li H, Liu H, Sage C, Huang M, Chen ZY, Heller S. 2004. Islet-1 expression in the developing chicken inner ear. J Comp Neurol 477:1–10.

Liu X, Mohamed JA, Ruan R. 2004. Analysis of differential gene expression in the cochlea and kidney of mouse by cDNA microarrays. Hear Res 197:35–43.

Lobo MK, Karsten SL, Gray M, Geschwind DH, Yang XW. 2006. FACS-array profiling of striatal projection neuron subtypes in juvenile and adult mouse brains. Nat Neurosci 9:443–452.

Lumpkin EA, Collisson T, Parab P, Omer-Abdalla A, Haeberle H, Chen P, Doetzlhofer A, White P, Groves A, Segil N, Johnson JE. 2003. *Math1*-driven GFP expression in the developing nervous system of transgenic mice. Gene Expr Patterns 3:389–395.

Mak AC, Szeto IY, Fritzsch B, Cheah KS. 2009. Differential and overlapping expression pattern of SOX2 and SOX9 in inner ear development. Gene Expr Patterns 9: 444–453.

Marsh ED, Minarcik J, Campbell K, Brooks-Kayal AR, Golden JA. 2008. FACS-array gene expression analysis during early development of mouse telencephalic interneurons. Dev Neurobiol 68:434–445.

Meighan-Mantha RL, Hsu DK, Guo Y, Brown SA, Feng SL, Peifley KA, Alberts GF, Copeland NG, Gilbert DJ, Jenkins NA, Richards CM, Winkles JA. 1999. The mitogen-inducible Fn14 gene encodes a type I transmembrane protein that modulates fibroblast adhesion and migration. J Biol Chem 274:33166–33176.

Meunier D, Peters T, Luttges A, Curfs J, Fundele R. 2003. Preferential expression of the G90 gene in post-mitotic cells during mouse embryonic development. Anat Embryol (Berl) 207:109–117.

Morris KA, Snir E, Pompeia C, Koroleva IV, Kachar B, Hayashizaki Y, Carninci P, Soares MB, Beisel KW. 2005. Differential expression of genes within the cochlea as defined by a custom mouse inner ear microarray. J Assoc Res Otolaryngol 6:75–89.

Morsli H, Choo D, Ryan A, Johnson R, Wu DK. 1998. Development of the mouse inner ear and origin of its sensory organs. J Neurosci 18:3327–3335.

Morsli H, Tuorto F, Choo D, Postiglione MP, Simeone A, Wu DK. 1999. *Otx1* and *Otx2* activities are required for the normal development of the mouse inner ear. Development 126:2335–2343.

Murga C, Laguinge L, Wetzker R, Cuadrado A, Gutkind JS. 1998. Activation of Akt/protein kinase B by G protein-coupled receptors. A role for alpha and beta gamma subunits of heterotrimeric G proteins acting through phosphatidylinositol-3-OH kinasegamma. J Biol Chem 273:19080–19085.

Nemoto Y, Chatani M, Inohaya K, Hiraki Y, Kudo A. 2008. Expression of marker genes during otolith development in medaka. Gene Expr Patterns 8:92–95.

Ozaki H, Nakamura K, Funahashi J, Ikeda K, Yamada G, Tokano H, Okamura HO, Kitamura K, Muto S, Kotaki H, Sudo K, Horai R, Iwakura Y, Kawakami K. 2004. *Six1* controls patterning of the mouse otic vesicle. Development 131:551–562.

Pourbakht A, Yamasoba T. 2003. Ebselen attenuates cochlear damage caused by acoustic trauma. Hear Res 181:100–108.

Powles N, Babbs C, Ficker M, Schimmang T, Maconochie M. 2004. Identification and analysis of genes from the mouse otic vesicle and their association with developmental subprocesses through in situ hybridization. Dev Biol 268:24–38.

Puligilla C, Dabdoub A, Brenowitz SD, Kelley MW. 2010. *Sox2* induces neuronal formation in the developing mammalian cochlea. J Neurosci 30:714–722.

Radde-Gallwitz K, Pan L, Gan L, Lin X, Segil N, Chen P. 2004. Expression of Islet1 marks the sensory and neuronal lineages in the mammalian inner ear. J Comp Neurol 477:412–421.

Raft S, Koundakjian EJ, Quinones H, Jayasena CS, Goodrich LV, Johnson JE, Segil N, Groves AK. 2007. Cross-regulation of Ngn1 and *Math1* coordinates the production of neurons and sensory hair cells during inner ear development. Development 134:4405–4415.

Rodriguez-Menocal L, St-Pierre M, Wei Y, Khan S, Mateu D, Calfa M, Rahnemai-Azar AA, Striker G, Pham SM, Vazquez-Padron RI. 2009. The origin of post-injury neointimal cells in the rat balloon injury model. Cardiovasc Res 81:46–53.

Rubel EW, Fritzsch B. 2002. Auditory system development: primary auditory neurons and their targets. Annu Rev Neurosci 25:51–101.

Sajan SA, Warchol ME, Lovett M. 2007. Toward a systems biology of mouse inner ear organogenesis: gene expression pathways, patterns and network analysis. Genetics 177: 631–653.

Sato T, Kawamura Y, Asai R, Amano T, Uchijima Y, Dettlaff-Swiercz DA, Offermanns S, Kurihara Y, Kurihara H. 2008. Recombinase-mediated cassette exchange reveals the selective use of Gq/G11-dependent and -independent endothelin 1/endothelin type A receptor signaling in pharyngeal arch development. Development 135:755–765.

Shi L, Reid LH, Jones WD, Shippy R, Warrington JA, Baker SC, Collins PJ, de Longueville F, Kawasaki ES, Lee KY, Luo Y, Sun YA, Willey JC, Setterquist RA, Fischer GM, Tong W, Dragan YP, Dix DJ, Frueh FW, Goodsaid FM, Herman D, Jensen RV, Johnson CD, Lobenhofer EK, Puri RK, Schrf U, Thierry-Mieg J, Wang C, Wilson M, Wolber PK, Zhang L, Amur S, Bao W, Barbacioru CC, Lucas AB, Bertholet V, Boysen C, Bromley B, Brown D, Brunner A, Canales R, Cao XM, Cebula TA, Chen JJ, Cheng J, Chu TM, Chudin E, Corson J, Corton JC, Croner LJ, Davies C, Davison TS, Delenstarr G, Deng X, Dorris D, Eklund AC, Fan XH, Fang H, Fulmer-Smentek S, Fuscoe JC, Gallagher K, Ge W, Guo L, Guo X, Hager J, Haje PK, Han J, Han T, Harbottle HC, Harris SC, Hatchwell E, Hauser CA, Hester S, Hong H, Hurban P, Jackson SA, Ji H, Knight CR, Kuo WP, LeClerc JE, Levy S, Li QZ, Liu C, Liu Y, Lombardi MJ, Ma Y, Magnuson SR, Maqsodi B, McDaniel T, Mei N, Myklebost O, Ning B, Novoradovskaya N, Orr MS, Osborn TW, Papallo A, Patterson TA, Perkins RG, Peters EH, Peterson R, Philips KL, Pine PS, Pusztai L, Qian F, Ren H, Rosen M, Rosenzweig BA, Samaha RR, Schena M, Schroth GP, Shchegrova S, Smith DD, Staedtler F, Su Z, Sun H, Szallasi Z, Tezak Z, Thierry-Mieg D, Thompson KL, Tikhonova I, Turpaz Y, Vallanat B, Van C, Walker SJ, Wang SJ, Wang Y, Wolfinger R, Wong A, Wu J, Xiao C, Xie Q, Xu J, Yang W, Zhang L, Zhong S, Zong Y, Slikker W,Jr. 2006. The MicroArray Quality

Control (MAQC) project shows inter- and intraplatform reproducibility of gene expression measurements. Nat Biotechnol 24:1151–1161.

Shin OH, Han W, Wang Y, Sudhof TC. 2005. Evolutionarily conserved multiple C2 domain proteins with two transmembrane regions (MCTPs) and unusual Ca2+ binding properties. J Biol Chem 280:1641–1651.

Smith CM, Finger JH, Hayamizu TF, McCright IJ, Eppig JT, Kadin JA, Richardson JE, Ringwald M. 2007. The mouse Gene Expression Database (GXD): 2007 update. Nucleic Acids Res 35:D618–623.

ten Berge D, Brouwer A, Korving J, Martin JF, Meijlink F. 1998. Prx1 and Prx2 in skeletogenesis: roles in the craniofacial region, inner ear and limbs. Development 125: 3831–3842.

Wassarman KM, Lewandoski M, Campbell K, Joyner AL, Rubenstein JL, Martinez S, Martin GR. 1997. Specification of the anterior hindbrain and establishment of a normal mid/hindbrain organizer is dependent on *Gbx2* gene function. Development 124:2923–2934.

Wu DK, Oh SH. 1996. Sensory organ generation in the chick inner ear. J Neurosci 16:6454–6462.

Additional Supporting Information may be found in the online version of this article.

CNE_22468_sm_suppinfoFigureS1.tif

Figure S1 EGFP expression in the LSCC, PSCC, utricle, saccule, SAG, cochlea, and endolymphatic duct of Line-14 mice at E12.5. (A-C) A section from the E12.5 LSCC and utricle in Line-14 mice (A,B) and its schematic view (C). Weak EGFP expression was detected in LSCC hair cells, which was confirmed by double staining with GFP (green) and Myo7a (magenta). In the utricle, EGFP expression was detected in the hair cells. (D-F) A section from the E12.5 PSCC (D,E) in Line-14 mice and its schematic view (F). EGFP expression was not detected in PSCC hair cells. (G-I) A section from the E12.5 saccule (G,H) and SAG in Line-14 mice and its schematic view (I). EGFP expression was detected in the saccule including hair cells, which was confirmed by double staining with GFP (green) and Myo7a (magenta). (J,K) A section from the E12.5 cochlea in Line-14 mice (J) and its schematic view (K). (L,M) A section from the E12.5 endolymphatic duct in Line-14 mice (L) and its schematic view (M). LC: lateral crista, UM: utricular macula, PC: posterior crista, SAG: statoacoustic ganglion, CD: cochlear duct, ED: endolymphatic duct, D: dorsal, L: lateral. Scale bars: 20 μm (A,B,D,E,G,H,L), 50 μm (J).

CNE_22468_sm_suppinfoFigureS2.tif

Figure S2 EGFP expression in the LSCC, PSCC, utricle, cochlea, and the endolymphatic duct of Line-14 mice at E13.5. Apart from the continuing EGFP-positive region (cochlea, saccule, and endolymphatic duct), EGFP-positive cells existed in each SCC and the utricle. (A-C) A section from the E13.5 LSCC in Line-14 mice (A,B) and its schematic view (C). EGFP expression was detected in LSCC hair cells, which was confirmed by double staining with GFP (green) and Myo7a (magenta). (D-F) A section from the E13.5 PSCC in Line-14 mice (D,E) and its schematic view (F). EGFP expression was detected in PSCC hair cells, which was confirmed by double staining with GFP (green) and Myo7a (magenta). (G-I) A section from the E13.5 utricle in Line-14 mice (G,H) and its schematic view (I). EGFP expression was detected in utricular hair cells, which was confirmed by double staining with GFP (green) and Myo7a (magenta). (J,K) A section from the E13.5 cochlea in Line-14 mice (J) and its schematic view (K). (L,M) A section from the E13.5 endolymphatic duct in Line-14 mice (L) and its schematic view (M). LC: lateral crista, PC: posterior crista, UM: utricular macula, CD: cochlear duct, ED: endolymphatic duct, D: dorsal, L: lateral. Scale bars: 20 μm (A,B,D,E,G,H,L), 50 μm (J).

CNE_22468_sm_suppinfoFigureS3.tif

Figure S3 EGFP expression in the vestibular and cochlear end organs and the endolymphatic duct of Line-14 mice at E15.5. (A-C) A section from the E15.5 ASCC in Line-14 mice (A,B) and its schematic view (C). EGFP expression was detected in ASCC hair cells, which was confirmed by double staining with GFP (green) and Myo7a (magenta). (D-F) A section from the E15.5 LSCC in Line-14 mice (D,E)

and its schematic view (F). EGFP expression was detected in LSCC hair cells, which was confirmed by double staining with GFP (green) and Myo7a (magenta). (G-I) A section from the E15.5 PSCC in Line-14 mice (G,H) and its schematic view (I). EGFP expression was detected in PSCC hair cells, which was confirmed by double staining with GFP (green) and Myo7a (magenta). (J-L) A section from the E15.5 utricle in Line-14 mice (J,K) and its schematic view (L). EGFP expression was detected in utricular hair cells, which was confirmed by double staining with GFP (green) and Myo7a (magenta). (M-O) A section from the E15.5 saccule in Line-14 mice (M,N) and its schematic view (O). EGFP expression was detected in the saccule including hair cells, which was confirmed by double staining with GFP (green) and Myo7a (magenta). (P,Q) A section from the E15.5 cochlea in Line-14 mice (P) and its schematic view (Q). The magnified image of the basal turn (arrow in P) is shown in Figure 3G,H. (R,S) A section from the E15.5 endolymphatic duct in Line-14 mice (R) and its schematic view (S). AC: anterior crista, LC: lateral crista, PC: posterior crista, UM: utricular macula, SM: saccular macula, CD: cochlear duct, ED: endolymphatic duct, D: dorsal, L: lateral. Scale bar: 20 μm (A,B,D,E,G,H,J,K,M,N,R), 50 μm (P).

CNE_22468_sm_suppinfoFigureS4.tif

Figure S4 EGFP expression in the ASCC, PSCC, utricle, and saccule of Line-14 mice at P2. (A-C) A section and its neighboring section from the P2 ASCC in Line-14 mice. EGFP expression was detected in ASCC hair cells, which was confirmed by double staining with GFP (green) and Myo7a (magenta). EGFP expression was also detected in some ASCC supporting cells (bracket in C), which was confirmed by double staining with GFP (green) and p27kip1 (magenta). (D-F) A section and its neighboring section from the P2 PSCC in Line-14 mice. EGFP expression was detected in PSCC hair cells, which was confirmed by double staining with GFP (green) and Myo7a (magenta). (G-I) A section and its neighboring section from the P2 utricle in Line-14. EGFP expression was detected in utricular hair cells, which was confirmed by double staining with GFP (green) and Myo7a (magenta). EGFP expression was also detected in some utricular supporting cells (bracket in I), which was confirmed by double staining with GFP (green) and p27kip1 (magenta). (J-L) A section and its neighboring section from the P2 saccule in Line-14 mice. EGFP expression was detected in saccular hair cells, which was confirmed by double staining with GFP (green) and Myo7a (magenta). EGFP expression was also detected in some saccular supporting cells (bracket in L), which was confirmed by double staining with GFP (green) and p27kip1 (magenta). AC: anterior crista, PC: posterior crista, UM: utricular macula, SM: saccular macula, D: dorsal, L: lateral. Scale bar: 20 μm.

CNE_22468_sm_suppinfoFigureS5.tif

Figure S5 EGFP expression in the ASCC, PSCC, utricle, saccule, and cochlea of Line-14 mice at P9. (A,B) A section from the P9 ASCC in Line-14 mice. EGFP expression was detected in ASCC hair cells, which was confirmed by double staining with GFP (green) and Myo7a (magenta). EGFP signals in some hair cells (bracket in A) weakened. (C,D) A section from the P9 PSCC in Line-14 mice. EGFP

expression was detected in PSCC hair cells, which was confirmed by double staining with GFP (green) and Myo7a (magenta). EGFP signals in some hair cells (bracket in C) weakened. (E,F) A section from the P9 utricle in Line-14 mice. EGFP expression was detected in utriclar hair cells, which was confirmed by double staining with GFP (green) and Myo7a (magenta), but EGFP signals in many hair cells weakened. (G,H) A section from the P9 saccule in Line-14 mice. EGFP expression was detected in saccular hair cells, which was confirmed by double staining with GFP (green) and Myo7a (magenta). (I,J) A section from the P9 cochlea in Line-14 mice. EGFP expression was detected in the inner and outer hair cells, which was confirmed by double staining with GFP (green) and Myo7a (magenta). EGFP expression was also detected in the inner sulcus cells (arrow in J) and inner phalangeal cells (arrowhead in J). AC: anterior crista, PC: posterior crista, UM: utricular macula, SM: saccular macula, OC: organ of Corti, D: dorsal, L: lateral. Scale bar: 20 μm.

CNE_22468_sm_suppinfoFigureS6.tif

Figure S6 ABR threshold (mean ± SD) at each tested frequency in homozygous, heterozygous, and wild-type mice at the age of 8 months (n = 5 each). There were no significant threshold differences among homozygous, heterozygous, and wild-type mice in each frequency according to the results of one-way ANOVA test (See Table S1).

CNE_22468_sm_suppinfoFigureS7.tif

Figure S7 Isolation of the heterozygous Line-14 EGFP-positive otocyst cells in E10.5 by FACS. (A) Light-scattering gate to exclude cell clumps and debris based on the parameters (size, forward-scattered light; granularity, side-scattered light). Only cells that fell within the defined gate in the light-scatter plot (gate R1) were subsequently analyzed for fluorescent expression. (B) Fluorescence intensity scatter plot of wild-type non-GFP cells. Wild-type non-GFP cells were used to identify a population of autofluorescent cells (gate R2). (C) Fluorescence intensity scatter plot of Line-14 otocyst cells. The scatter plot in B was compared with the profiles of cells from transgenic mice to define the GFP sorting window. EGFP-positive cells (gate R3) and EGFP-negative cells (gate R2) were then gated. Nonviable cells were excluded by staining with PI.

CNE_22468_sm_suppinfoTableS1.tif

Supporting Information Table 1

CNE_22468_sm_suppinfoTableS2.tif

Supporting Information Table 2

Figure S1

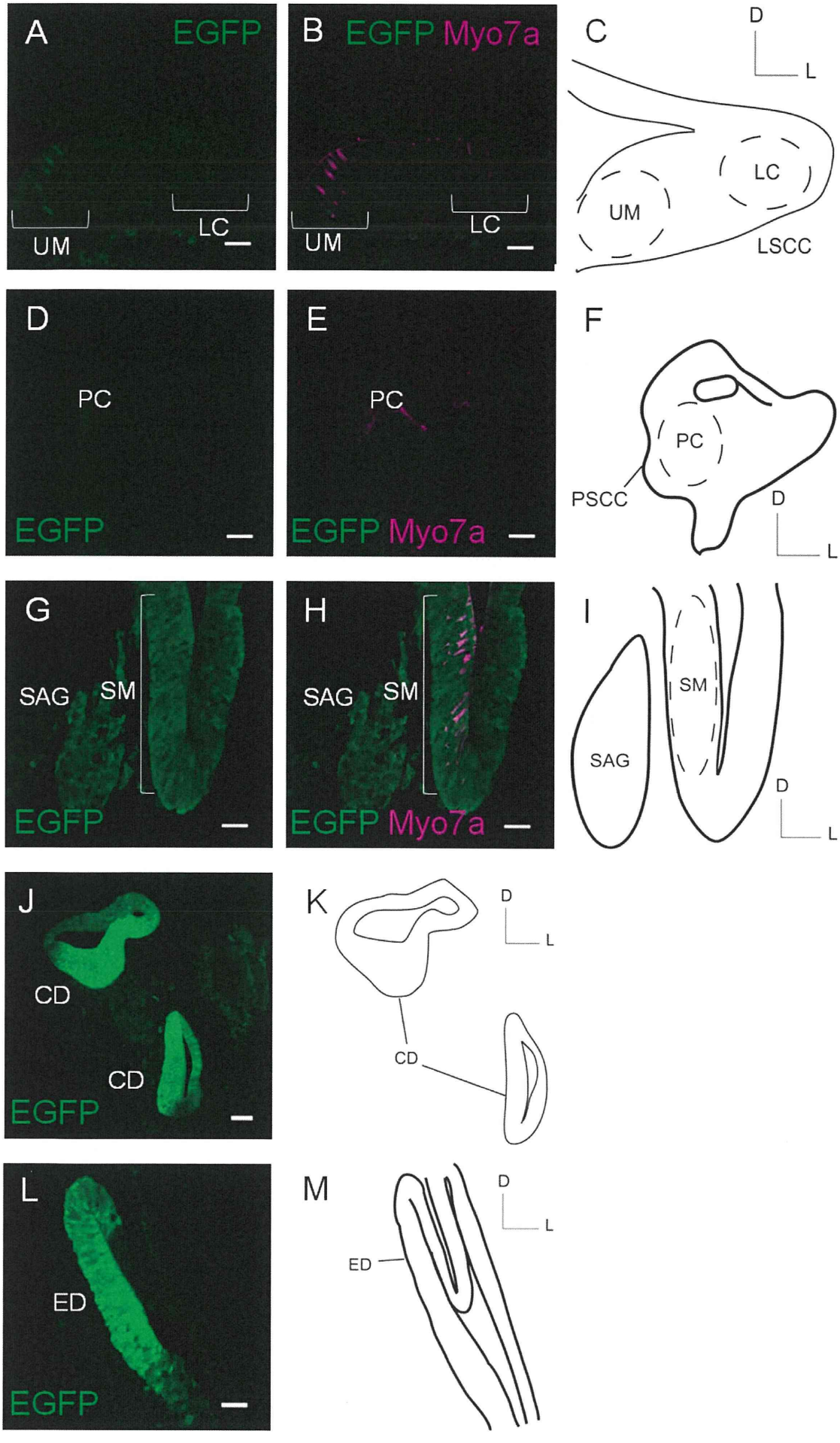
A
EGFP
UM
LC
B
EGFP Myo7a
UM
LC
C
D
L
LC
UM
LSCC
D
PC
EGFP
E
PC
EGFP Myo7a
F
PC
PSCC
D
L
G
SAG
SM
EGFP
H
SAG
SM
EGFP Myo7a
I
SM
SAG
D
L
J
CD
CD
EGFP
K
D
L
CD
L
L
EGFP
M
D
L
ED

Figure S2

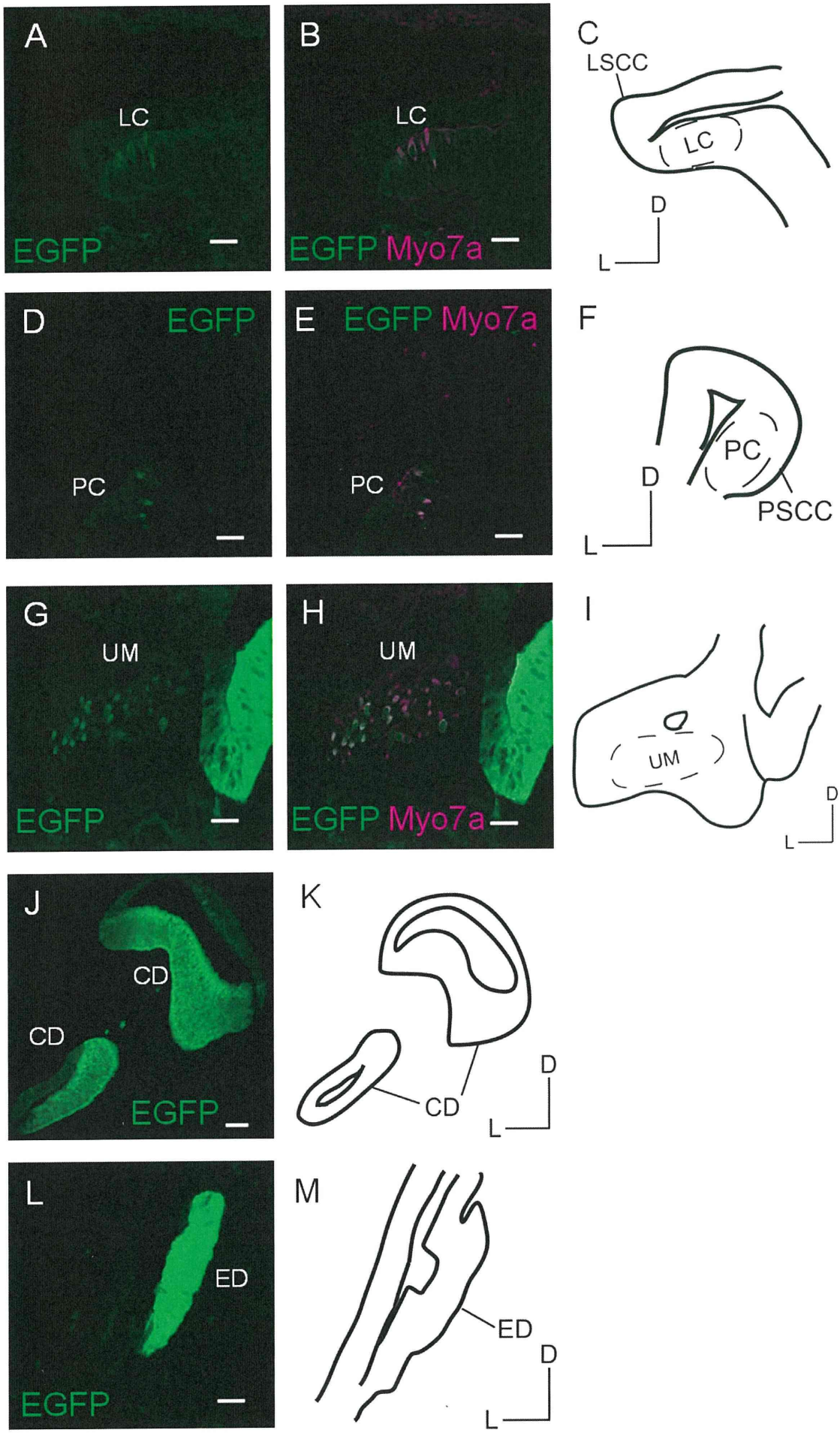
A
LC
EGFP
B
LC
EGFP Myo7a
C
LSCC
LC
D
L
D
EGFP
PC
E
EGFP Myo7a
PC
F
PC
D
PSCC
L
G
UM
EGFP
H
UM
EGFP Myo7a
I
UM
D
L
J
CD
CD
EGFP
K
CD
D
L
L
ED
EGFP
M
ED
D
L

Figure S3

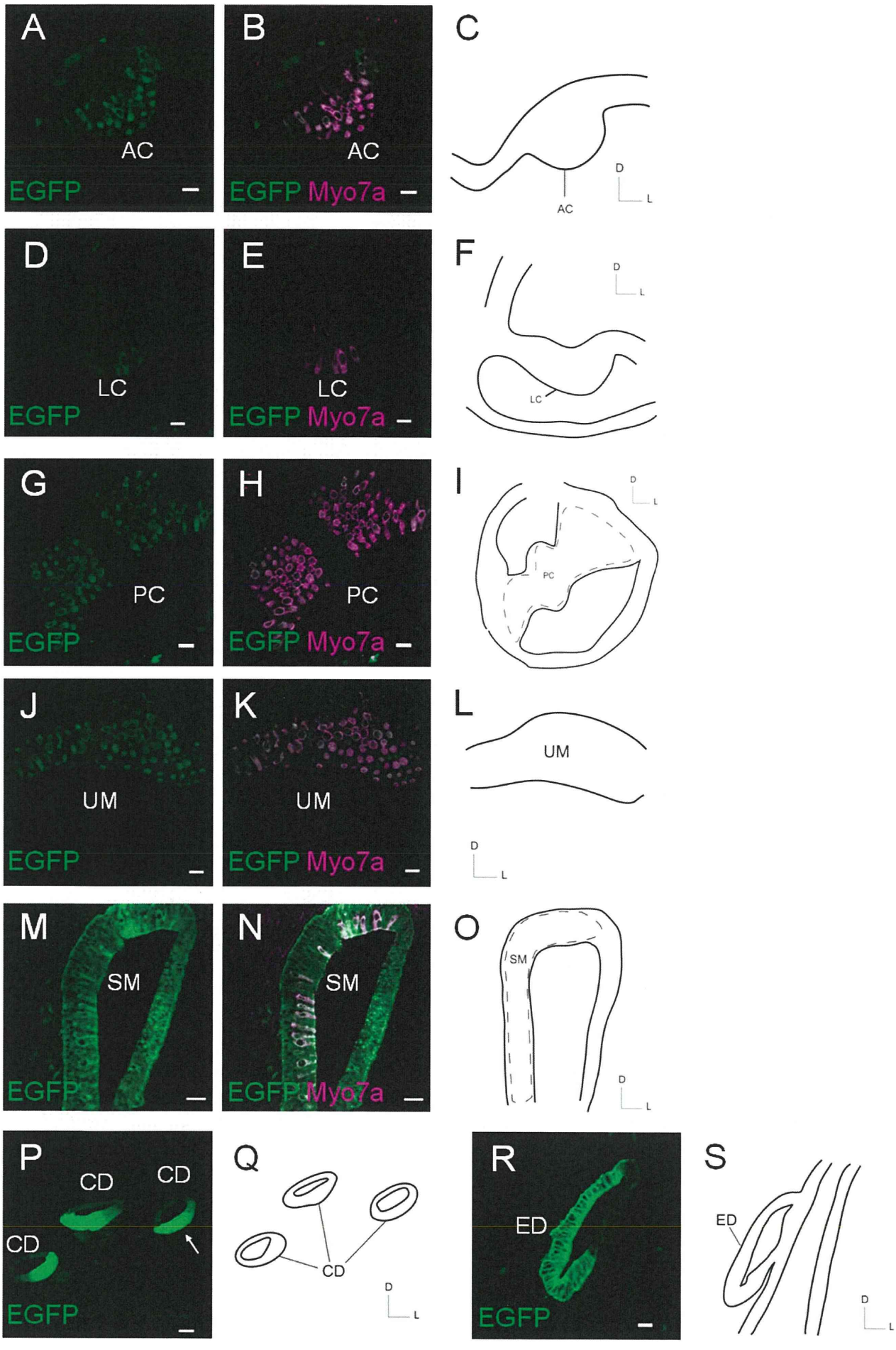
A
AC
EGFP
B
AC
EGFP Myo7a
C
AC
D
L
D
LC
EGFP
E
LC
EGFP Myo7a
F
LC
G
PC
EGFP
H
PC
EGFP Myo7a
I
PC
J
UM
EGFP
K
UM
EGFP Myo7a
L
UM
M
SM
EGFP
N
SM
EGFP Myo7a
O
SM
P
CD
CD
CD
EGFP
Q
CD
R
ED
EGFP
S
ED

Figure S4

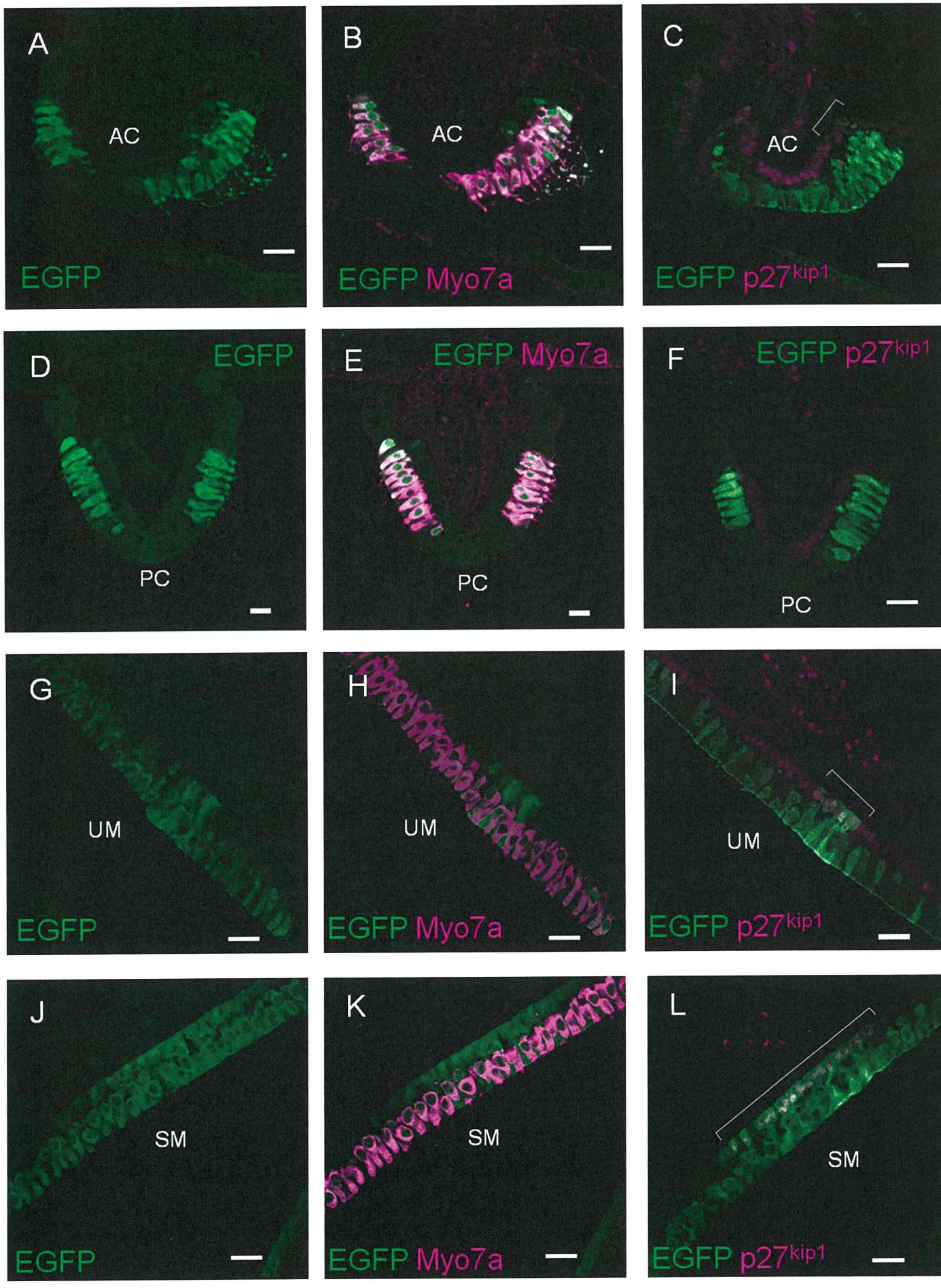
A
AC
EGFP
B
AC
EGFP Myo7a
C
AC
EGFP p27kip1
D
EGFP
PC
E
EGFP Myo7a
PC
F
EGFP p27kip1
PC
G
UM
EGFP
H
UM
EGFP Myo7a
I
UM
EGFP p27kip1
J
SM
EGFP
K
SM
EGFP Myo7a
L
SM
EGFP p27kip1

Figure S5

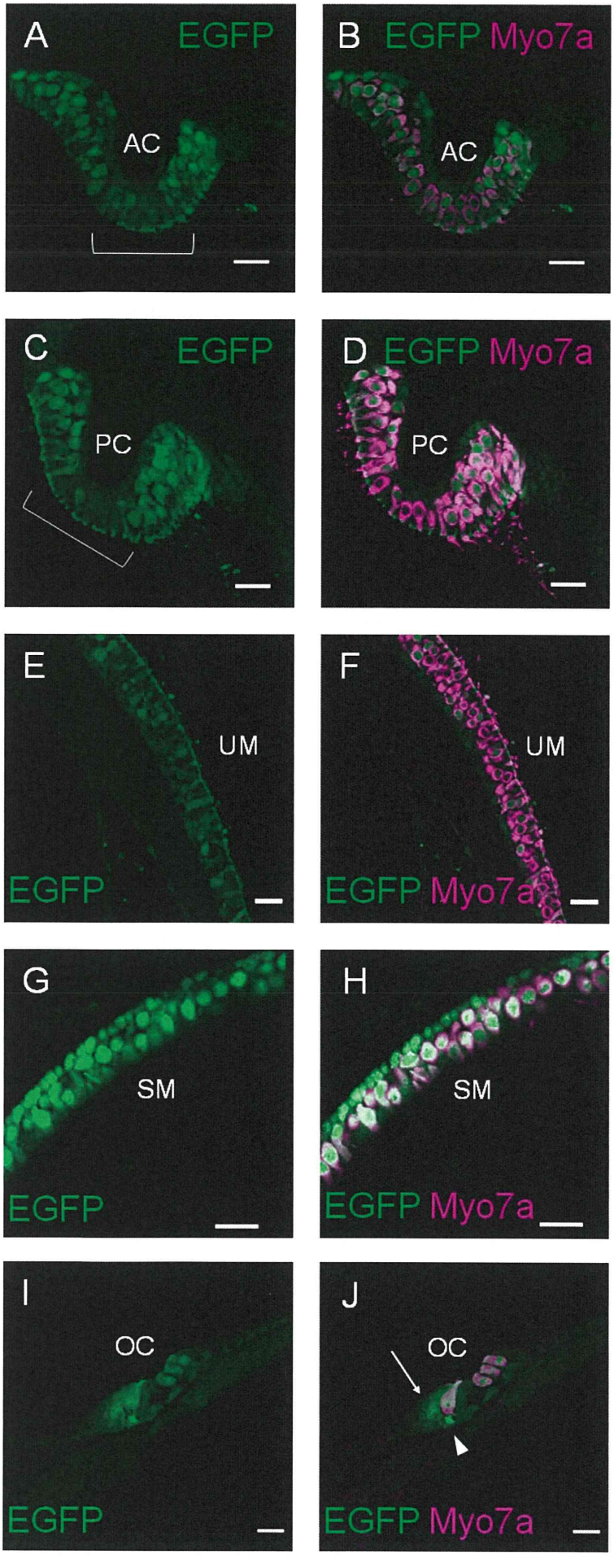
A
EGFP
AC
B
EGFP Myo7a
AC
C
EGFP
PC
D
EGFP Myo7a
PC
E
UM
EGFP
F
UM
EGFP Myo7a
G
SM
EGFP
H
SM
EGFP Myo7a
I
OC
EGFP
J
OC
EGFP Myo7a

Figure S6

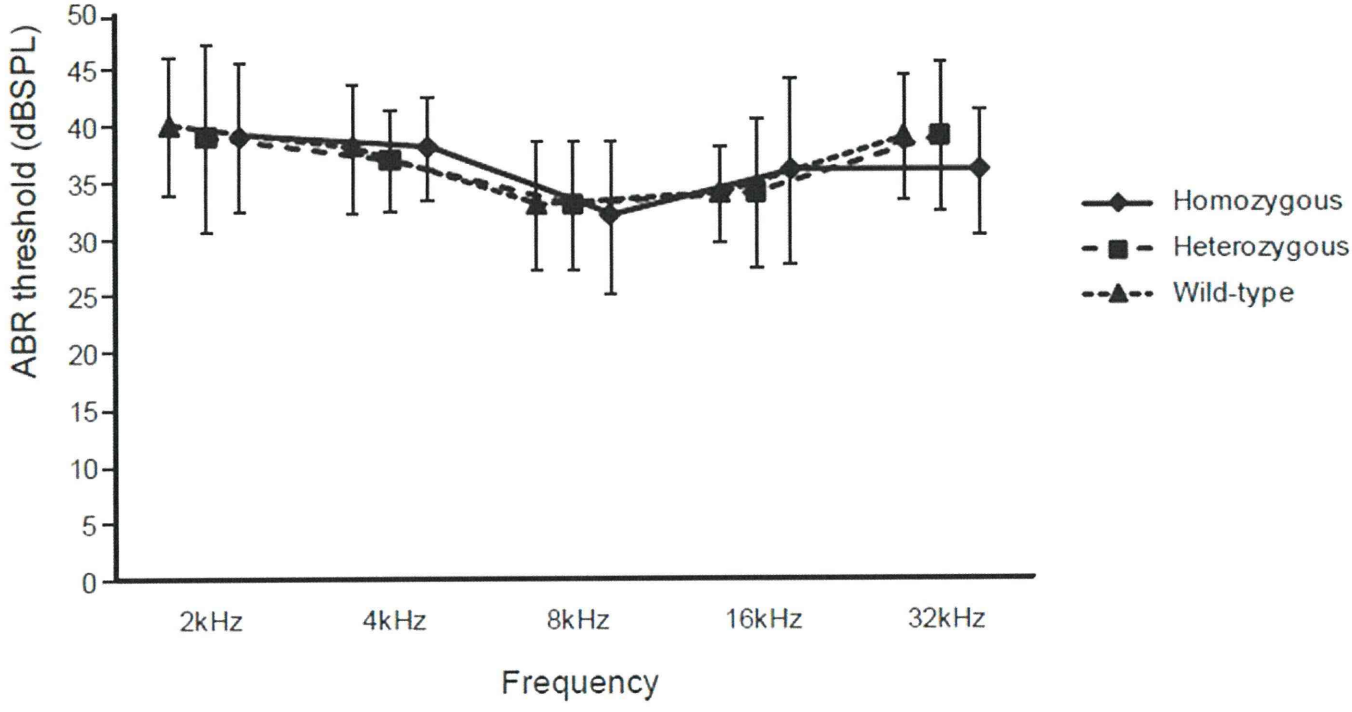
ABR threshold (dBSPL)
50
45
40
35
30
25
20
15
10
5
0
2kHz
4kHz
8kHz
16kHz
32kHz
Frequency
Homozygous
Heterozygous
Wild-type